

A Novel Method of Resistance for Influenza Against a Channel-Blocking Antiviral Drug

Peleg Astrahan,¹ Itamar Kass,¹ Matthew A. Cooper,^{2†} Isaiah T. Arkin^{1*}

¹Department of Biological Chemistry, Alexander Silberman Institute of Life Sciences, Hebrew University, Jerusalem, Israel

²Department of Chemistry, University of Cambridge, Cambridge, United Kingdom

ABSTRACT Effective antivirals are few and far between, and as such, the appearance of resistance toward such treatments is an obvious medical concern. In this article, we analyze the mechanism by which influenza attains resistance toward amantadine, a blocker of the viral M2 H⁺ channel. Binding analyses of amantadine to M2 peptides from different viral strains showed that the virus has developed two alternate routes to avoid blockage of its channel: (1) a conventional route, in which the channel no longer binds the blocker and, hence, the blocker cannot exert its inhibitory function; and (2) a novel mechanism, in which binding of the blocker is retained, yet the function of the protein is unaffected. Pore diameter profiles revealed the molecular mechanism by which the virus may attain this novel type of resistance: an increase in the size of the channel. Thus, despite the drug binding the channel, it may not be able to block the pore, since the channel diameter has increased. Our findings may have broad ramifications in the design of new antivirals, and of novel blockers against malfunctioning human channels implicated in disease. *Proteins* 2004;55:251–257. © 2004 Wiley-Liss, Inc.

Key words: ion channel; influenza; antiviral; protein structure; channel blocker

INTRODUCTION

As the causative agent of one of the deadliest infectious diseases, influenza presents an obvious target for pharmaceutical point intervention. Currently in prophylactic use are two classes of anti-influenza agents: those that inhibit the viral neuraminidase and those that block the M2 H⁺ channel. Viral resistance toward these agents is on the increase,^{1,2} more so in the case of M2 blockers.³ Clearly, proper understanding of the molecular basis of resistance is of paramount biomedical importance. Furthermore, insight into the M2-amantadine system may serve as a paradigm for other channel-blocker systems that are far less understood.

The M2 protein is encoded by the spliced mRNA segment 7 of the Influenza A virus,⁴ and includes a 24-residue N-terminal extracellular domain, a 19-residue hydrophobic transmembrane domain, and a 54-residue cytoplasmic tail.⁵ M2 forms a homotetrameric transmembrane α -helical bundle⁶ that acts as a H⁺ channel.⁷ The channel is closed at physiological pH and is activated at pH \leq 6.2, a

function attributed to the H37 residue located in the channel pore.⁸ M2's H⁺ channel activity is crucial to the virus life cycle in two aspects: First, following virus endocytosis and endosome acidification, M2 is activated and results in the concomitant acidification of the virus lumen. This acidification weakens the bonds between the viral RNA and the virus capsid. Second, during virus exit, M2's H⁺ channel activity ensures that the exosome does not acidify. This prevents the untimely, acid-triggered, irreversible conformational change of the viral hemagglutinin. Based on the above observations, it is obvious that any molecule that blocks the M2 channel would be an effective anti-influenza agent.

Amantadine (1-aminoadamantane) is a 188-Da polycyclic amine that inhibits the replication of Influenza A. The clinical usage of amantadine has been rather limited since the 1960s, due to several side effects and the appearance of amantadine-resistant viral strains.³ That the viral target of amantadine is M2 was proven in a landmark study,⁹ in which amantadine-resistant mutants of influenza viruses were shown to contain single amino acid substitutions in the M2 protein. The mutations that conferred amantadine resistance localized to the transmembrane domain of the protein at one of four amino acid sites: 27, 30, 31, and 34. Finally, in another seminal study,⁷ upon identifying M2 as a H⁺ channel, the molecular basis of amantadine's function was identified as a specific blocker of the M2 channel.

Structurally, both solid-state NMR^{10–12} and site-specific Fourier transform infrared (FTIR) dichroism analysis¹³ were able to determine the tilt and rotational pitch angles of the helices in the tetrameric transmembrane bundle, which constitutes a functional channel. More recently, distance restraints from solid-state NMR studies refined the current backbone structure of M2.¹⁴ The structural data positioned the amino acids whose mutations generated resistance to amantadine (sites 27, 30, and 34) as facing the pore of the channel (Fig. 1). The amino acid in site 31 is partially in the protein–protein interface and

Grant sponsor: Israel Science Foundation; Grant number: 784/01 to ITA.

*Correspondence to: Isaiah T. Arkin, Hebrew University, Biological Chemistry, Givat Ram Campus, Jerusalem 91904, Israel. E-mail: arkin@cc.huji.ac.il

†Present address: Akubio Limited, 181 Cambridge Science Park, Cambridge, CB4 0GJ, UK.

Received 3 June 2003; Accepted 17 September 2003

Published online 16 March 2004 in Wiley InterScience (www.interscience.wiley.com). DOI: 10.1002/prot.20018

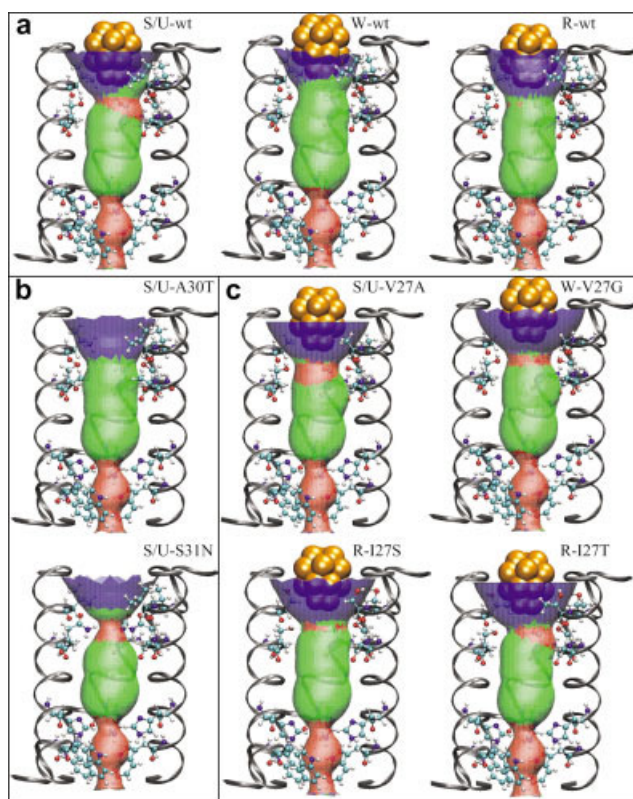


Fig. 1. Molecular representation of the M2 pore according to the structure available from solid state NMR studies.¹⁴ Amantadine, shown in orange Corey-Pauling-Koltun (CPK) representation is provided in order to gain reference as to the relative sizes of the pore and its cognate blocker. At this time, the exact position and manner by which amantadine binds the pore is not known. Color coding is according to pore diameter: red, 2–3 Å; green, 3–4 Å; and blue, 4–5 Å calculated by the program HOLE¹⁹ and depicted with the program VMD.²⁶ Note that the pore diameter is measured from a line representing the bundle axis. Since the model may not be perfectly symmetric, the pore diameter is likewise not perfectly centrically symmetric. Residues V27, A30, S31 (according to Singapore strain) that have undergone mutations yielding resistance to amantadine, as well as the two residues implicated in channel activation and gating, H37 and W41^{8,20} are shown in ball-and-stick representation. **Panel a:** wild-type, amantadine-sensitive strains, whereby S/U, W, and R stand for Singapore/udron, Weybridge and Rostock viral strains, respectively. **Panel b:** amantadine-resistant mutant strains that have lost the ability to bind amantadine. **Panel c:** amantadine-resistant mutant strains that retain amantadine binding. Note the increased pore size of mutants in Panel c (that retain binding) relative to the wild-type strains, and the decreased pore size of Singapore/udron S31N mutant in Panel b that does not bind amantadine.

partially in the pore. The stage is thus set for a detailed molecular analysis of amantadine's mode of inhibition.

MATERIAL AND METHODS

Synthetic peptides corresponding to the predicted transmembrane domain of the M2 and three adjacent amino acids from each side were made by W. M. Keck Biotechnology Resource Center (New Haven CT). The sequences of the peptides are given in Figure 2. The peptides were dissolved in trifluoroacetic acid (TFA) and injected into a Jupiter 5 μ c4 300 Å reverse-phase high performance liquid chromatography (HPLC) column (Phenomenex). Peptides were eluted from the column with a 30-min linear gradient

Sing./Udron	SSDPLVVAASIIIGILHLILWILDRL
Weybridge	SSDPLVIAASIIIGILHFILWILDRL
Rostock	SSDPLIIAASIIIGILHLILWILNRL
Sing./Udron	SSDPLVVAASIIIGILHLILWILDRL
Val27Ala	SSDPLAVAASIIIGILHLILWILDRL
Ala30Thr	SSDPLVVATSIIGILHLILWILDRL
Ser31Asn	SSDPLVVAANIIGILHLILWILDRL
Weybridge	SSDPLVIAASIIIGILHFILWILDRL
Val27Gly	SSDPLGIAASIIIGILHFILWILDRL
Rostock	SSDPLIIAASIIIGILHLILWILNRL
Ile27Ser	SSDPLSIAASIIIGILHLILWILNRL
Ile27Thr	SSDPLTIAASIIIGILHLILWILNRL

Fig. 2. Sequences of the M2 transmembrane domain peptides used in the amantadine binding study.¹⁸ **Top panel:** difference between the different viral strains. Marked in purple, blue, and green are residues unique to Singapore/udron, Weybridge and Rostock strains, respectively. Note that the transmembrane domain of Udron strain is identical to that of Singapore. All of the wild-type strains are sensitive to amantadine. **Bottom panels** indicate the different amantadine-resistant mutants and their respective "wild-type" strains. Sites in which differences occur between the mutant, amantadine resistant strain and its amantadine-sensitive, wild-type parent strain, are marked in red.

from 20% to 100% organic phase (2:3 acetonitrile:isopropanol). All solvent contained 0.1% TFA. Finally, the eluted fraction containing pure peptide were lyophilized.

Approximately 1 mg of lyophilized peptide and 10 mg of 1,2-dimyristoyl-sn-glycero-3-phosphocholine (Avanti polar lipids) were dissolved in 900 μ L hexafluoro-2-propanol. The solution was mixed at 37°C for 1 h, until the hexafluoro-2-propanol had evaporated completely. The protein–lipid mixture was dissolved in twice-filtered phosphate-buffered saline (PBS), pH 7.4 (10 mM Na₂HPO₄ · NaH₂PO₄, 120 mM NaCl and 2.7 mM KCl) to a final lipid concentration of 3 mM. The solution was mixed for another 20 min, yielding a white suspension of M2TMP reconstituted liposomes. The M2TMP reconstitution was confirmed by FTIR spectroscopy, focusing on the analysis of dichroic ratios, as outlined elsewhere.¹³

The liposomes were inserted into Spectra/por 2 cellulose dialysis bags, 12,000–14,000 Da molecular weight cutoff, and mixed for 30 min in PBS, bringing the solution on both sides of the liposomes membrane into equilibrium. Resizing the liposomes to a unified size of 0.1 μ m was achieved by extruding the liposomes (dissolved in PBS) through an Avanti Mini Extruder (Avanti polar lipids) with 0.1 μ m polycarbonate membranes (19 mm in diameter).

The binding measurements were made on a Biacore 3000 system, with the L1 chip as the experiment's surface. The L1 chip (2.4 × 0.5 × 0.05 mm—l × w × h) contains carboxymethyl dextran hydrogel residues, allowing the binding of liposomes to the surface.¹⁵ The L1 chip was cleaned prior to each experiment with the detergent 2-cyclohexylaminopropanesulfonic acid (CHAPS) 20 mM,

in a volume of 40 μL and a flow rate of 20 $\mu\text{L}/\text{min}$. Immediately after cleaning the cells, the liposomes were immobilized on the chip (80 μL at a flow rate of 2 $\mu\text{L}/\text{min}$). Excess of unbound liposomes were removed by flowing 10 mM NaOH in PBS (50 μL at a flow rate of 100 $\mu\text{L}/\text{min}$) followed by PBS injection for 4 h at a rate of 5 $\mu\text{L}/\text{min}$.

The binding analysis included the injection of two-fold dilutions of amantadine (60 μL at a flow rate of 20 $\mu\text{L}/\text{min}$) in the concentration range of 70 μM –10 mM on the chip (immobilized with M2TMP reconstituted liposomes). At the end of the amantadine injection, after the system reached equilibrium [resonance units (RUs) ceased to increase], the system was allowed to dissociate for 1 min in PBS (flow rate of 20 $\mu\text{L}/\text{min}$). Subsequently, the surface was regenerated by 10 mM HCl (10 μL at a flow rate of 20 $\mu\text{L}/\text{min}$). Complete removal of the liposomes was achieved by a second CHAPS injection (40 μL at a flow rate of 20 $\mu\text{L}/\text{min}$).

Each experiment included the immobilization of empty liposomes (i.e., those without protein) in one of the chip's cells, serving as a reference. The mean RUs of the last 15–10 s of amantadine injection on the empty liposome's cell were subtracted from the mean RU at the same time area (steady-state zone) in the M2TMP reconstituted liposomes cell.

The results were calibrated for "solvent effects" as described.¹⁶ This calibration is especially important when the experiment buffer's RU is high and has a refraction index that differs from that of the sample, which is common in cases involving low-molecular-weight analytes. The calibration factor for each injection's equilibrium RU, was produced from a calibration curve of $\text{RU}_{\text{Checked cell}} - \text{RU}_{\text{Reference cell}}$ versus $\text{RU}_{\text{Reference cell}}$ when different PBS concentrations were injected over the cells. Since the PBS does not bind to the cells, nor to the liposomes or to the M2TMP, it could reflect differences between the chip cells that are not due to binding.¹⁶

Due to the fact that the on- and off-rate constants of amantadine binding to M2TMP were rapid, all thermodynamic analyses were based on equilibrium, steady-state measurements (see below).

The binding results were represented as dose–response curves, in which the final RU_{eq} is plotted against the different amantadine concentrations. The dose–response curve was fitted to the diagram according to Eq. (4) (see Appendix) and the disassociation constant (KD) was derived using the Biaevaluation 3.0 program (Biacore). The goodness of fit was estimated as χ^2 values, where a good fit of a binding curve to a binding diagram is estimated as $\chi^2 < 10$.

In order to offset any effects due to different amounts of peptide bound to the chip, the calculated RU_{MAX} (see Appendix) was normalized, determining the goodness of fit, since it changes once the binding diagram is multiplied by a constant factor. By multiplying, we are actually simulating the same binding diagram, except with a different M2TMP concentration. However, since equilibrium constants such as KD do not change due to multiplication, the diagrams of all the M2TMPs were multiplied by

different factors, bringing their estimated R_{MAX} together to the same RU (this procedure is similar to calibrating the M2TMP concentration). The fitting curve program was then run once again to produce the calibrated χ^2 . This procedure allows us to compare the different M2TMPs χ^2 , and determine whether the M2TMP reconstituted liposomes bind amantadine (i.e., has $\chi^2 < 10$) or not $\chi^2 > 10$.

The model used to analyze the surface plasmon resonance (SPR) data assumed a 1:1 binding stoichiometry between amantadine and M2TMP, and is described in detail in the Appendix.

RESULTS AND DISCUSSION

In order to gain insight into the molecular mechanism of resistance toward amantadine, we measured the binding of amantadine to peptides encompassing the transmembrane segment of M2 from amantadine-sensitive and resistant viral strains, using SPR, employing a polymer cushion supported lipid bilayer. We note that the mutants selected are natural variants of the virus. Since the channel activity of the M2 tetramer is vital to the virus life cycle, it is possible to conclude that any mutation studied ablates amantadine channel blocking function, while preserving tetramerization and channel function of M2.

The sequences of the different peptides analyzed are shown in Figure 2. Note that the sequence of transmembrane segments of udorn and Singapore strains are identical. The transmembrane peptides used were shown to be necessary, and sufficient, to represent all of the activities and specificity of M2 with respect to channel properties and amantadine inhibition.¹⁷

Figure 3(a) depicts the amantadine dose–response curves obtained under equilibrium conditions for three wild-type, amantadine-sensitive virus strains. The data were fitted using a model describing the binding of one molecule of amantadine to one channel, yielding the affinity constants listed in Figure 3. The values obtained indicate that Singapore/udorn strains have a higher affinity for amantadine versus Rostock and Weybridge strains. The experimental variation does not facilitate an accurate distinction between the affinities of Rostock and Weybridge strains for amantadine.

The above results are consistent with viral sensitivity toward amantadine, in that Singapore/udorn strains exhibit the highest sensitivity, followed by Rostock and Weybridge strains.¹⁸ Furthermore, the trend reflecting the increased affinity for amantadine of Singapore/udorn versus Rostock and Weybridge strains, is consistent with previously measured "apparent isochronic inhibitory binding constants."¹⁸

The apparent isochronic inhibitory binding constants obtained by Lamb and coworkers¹⁸ are significantly lower than the equilibrium binding constants obtained in the current study. However, they cannot be compared to the results obtained herein, due to the following reasons:

- The apparent isochronic inhibitory binding constants measured by Lamb and coworkers¹⁸ were obtained after adding amantadine in various concentrations and mea-

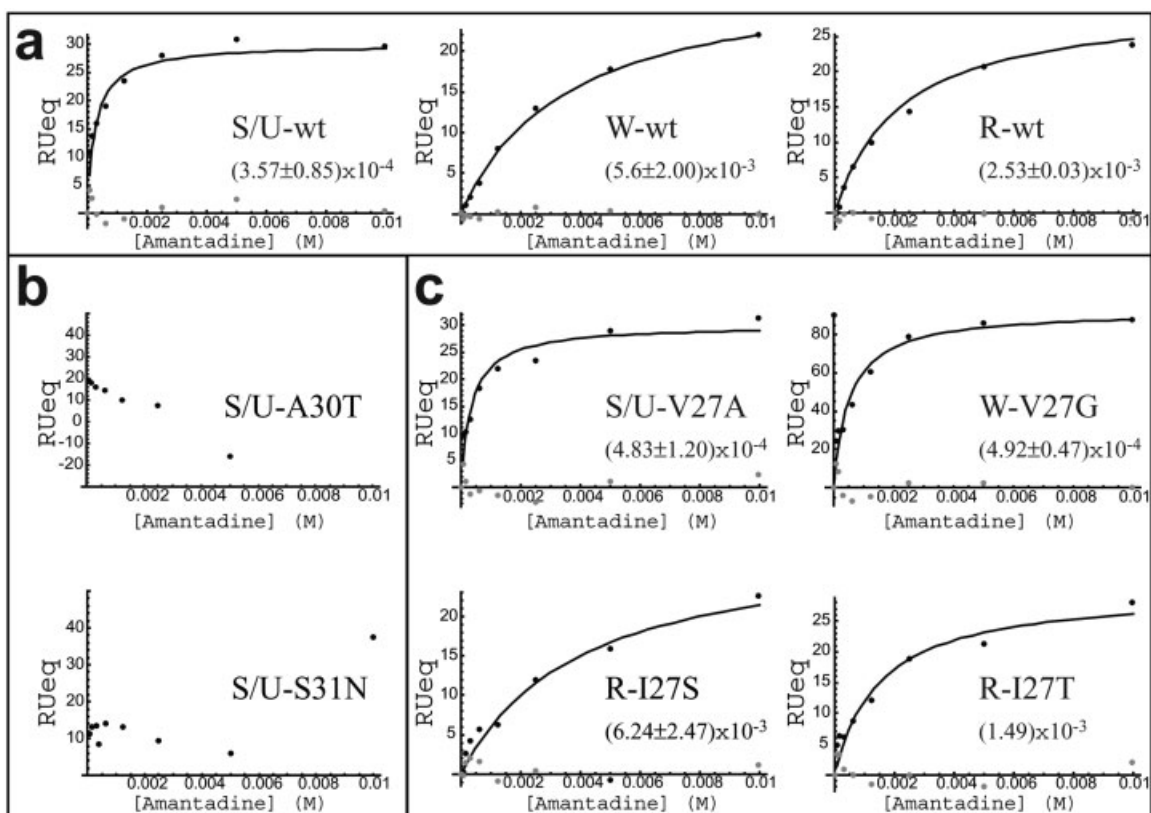


Fig. 3. Representative amantadine SPR dose response curves. The data, shown in solid circles, were fitted (solid line) using nonlinear regression to a model describing the binding of one molecule of amantadine to one channel in one step. The residuals (i.e., differences between the data and the fit) are shown in gray. **Panel a:** wild-type, amantadine-sensitive strains, whereby S/U, W, and R stand for Singapore/udorn, Weybridge and Rostock viral strains, respectively. **Panel b:** amantadine-resistant mutant strains that have lost the ability to bind amantadine. **Panel c:** amantadine-resistant mutant strains that retain amantadine binding.

asuring the reduction in the current after a set amount of time (see below), not letting the system reach equilibrium. It is for this reason that the binding constants are classified as “isochronic apparent inhibitory binding constants” by the authors. In the current study, the binding constants are measured at equilibrium.

- The choice of the time point to measure nonequilibrium binding is critical and the value of the isochronic apparent inhibitory binding constants depends on it. Shorter times would lead to higher isochronic apparent inhibitory binding constants, while longer times would lead to lower isochronic apparent inhibitory binding constants. Perhaps if the time point used by Lamb and coworkers¹⁸ were shorter than the 2 min used, the correlation between the two studies would have been higher.
- Finally, the amantadine inhibition measured by Lamb and coworkers¹⁸ was irreversible. Thus, any binding constant measured should be much higher than that obtained under reversible conditions. It is therefore not surprising that the equilibrium binding constants obtained herein, under reversible conditions, were higher than the isochronic apparent inhibitory binding constants obtained by Lamb and coworkers under irreversible conditions. We note that the reversibility

of amantadine binding to M2 has been observed previously,¹⁷ with results similar to those obtained herein and in contrast to the results obtained by Lamb and coworkers.¹⁸

The amantadine dose–response curves obtained from two Singapore/udorn amantadineresistant strains, A30T and S31N, are shown in Figure 3(b). As expected, both mutants exhibited no binding of amantadine, indicating that resistance toward the channel blocker is most likely caused by the loss of affinity toward the drug. A different and surprising result is shown in Figure 3(c), in which four different mutants, originating from three viral strains, retain their amantadine binding capabilities, despite being resistant toward the drug. Our results indicate that the residues implicated in binding amantadine are located at positions 30 and 31, (not 27) thereby potentially mapping the drug binding site.

To the best of our knowledge, channels that lose functional sensitivity toward a particular blocker, yet remain able to bind it, have not been reported previously. Thus, the virus has developed two alternate routes to avoid blockage of its channel: (1) a conventional route in which the channel no longer binds the blocker and, hence, the blocker cannot exert its inhibitory function; and (2) a novel

mechanism in which binding of the blocker is retained, yet the function of the protein is not affected.

How can a channel retain binding of its cognate channel blocker, yet mutate so as to regain channel activity? One hypothesis that may explain the above finding arises from careful analysis of the nature of the mutations that take place. In the amantadine-resistant mutants that have lost the ability to bind amantadine [Fig. 3(b)], the mutations introduce a larger amino acid (S31 → N and A30 → T). The binding pocket for the drug may be occluded, or its chemical nature has been changed. The drug therefore can no longer bind due to steric hindrance, or chemical incompatibility. In the amantadine-resistant mutants that retain amantadine binding [Fig. 3(c)], the mutations introduce a smaller amino acid (V27 → G, I27 → S, I27 → T, and V27 → A). Thus, it is possible that in these mutants, amantadine can still bind the channel, but since the pore is larger, the channel is no longer blocked. Thus the virus may use two structural tactics to make a channel blocker ineffective: (1) reduce the diameter of the pore or change the chemical properties of the pore, so that in both cases the blocker does not bind, or (2) increase the pore diameter, so that even if the blocker binds, it will not block the channel.

Based on the backbone structure of the M2 transmembrane peptide solved in lipid bilayers by solid-state NMR,¹⁴ it was possible to computationally construct likely models for the different mutants and thus provide a molecular picture that is consistent with the above hypothesis. We proceeded to calculate the pore diameter along the axis of the channel¹⁹ of each of the structures, the results of which are shown in Figure 1.

The pore diameter profiles of all three amantadine-sensitive wild-type structures are similar [Fig. 1(a)]. The sites that are most restricted along the pore are in the vicinity of the two residues implicated in channel activation⁸ and gating,²⁰ H37 and W41, respectively. In relation to the pore diameter of M2, the size of amantadine would seem to fit well with its function as a channel blocker. Although no specific structural data are available to accurately place amantadine's whereabouts in the pore, size considerations alone suggestively maintain that it binds above the first restriction orifice in the channel. This is the exact point in which the residues that mutate to generate resistance to amantadine are located. For illustrative purposes, therefore, we placed amantadine slightly above this orifice in order to gauge the relative effects of the amino acid mutations.

Analysis of the pore profiles of those amantadine-resistant mutants that have retained amantadine binding is consistent with the above hypothesis. In all of the aforementioned mutants there is a significant increase in the pore diameter [Fig. 1(c)]. Moreover, the increase in pore diameter is located right above the first constriction, where amantadine might be located. Conversely, the Singapore/udorn M2 S31N mutant, which no longer binds amantadine, shows a clear reduction of the pore diameter, consistent with the fact that it cannot bind the channel blocking drug (Fig. 1, bottom of panel b). The mutant

Singapore/udorn M2 A30T that has lost binding of amantadine as well, does not show an appreciable reduction in pore size. Its loss of binding may be interpreted through alteration of the chemistry of the binding pocket (e.g. change of hydrophobicity due to the insertion of the threonine hydroxyl).

Both of the above examples are encouragingly consistent with the effects that pore diameter changes might have upon the susceptibility of the channel toward blockage. In gauging the differences observed, it is important to remember that the channel is thought to conduct H⁺'s by way of a H⁺ wire.^{21,22} A blocker that binds the channel may exert its channel-blocking activity by obstructing the continuous water molecule file, thereby eliminating the H⁺ wire. As such, small differences are all that are needed to reestablish this wire in the case of a mutant that retains amantadine binding. Indeed, our results point to the fact that the binding site for amantadine is located near residues 30 and 31, while the site in which the disruption of the water molecule file is alleviated is located in the vicinity of residue 27. That these two sites are distinct may explain how the M2 channel can mutate so as to retain drug binding, yet regain channel activity.

To the best of our knowledge, channels that lose sensitivity toward a particular blocker, yet remain able to bind it, have not been reported previously. A reciprocal case has, however, been reported: μ conotoxin, a potent skeletal muscle Na⁺ channel blocker. In this peptide, a mutation of arginine to smaller residues results in partial blockage of the channel.²³ Thus, in this instance, the blocker has potentially decreased in size and is therefore not able to completely block the channel.

Table 1 in Holsinger et al.²⁴ indeed shows that there is an attenuation in the pH activation for some mutants, the best example being A30T. However, for other mutations, such as S31N, this is not the case. These two mutants behave in our binding studies in an identical manner; in other words, both have lost the ability to bind the channel. It is therefore difficult to account for this loss of binding only though the attenuation in the pH activation, since only one of the mutants behaves in this way. In addition, the mutant V27A behaves indistinguishably from wt with respect to pH activation (as well as S31N) and is one of our set of mutants that retains amantadine binding. Thus no correlation can be made between attenuation in pH activation response and the affinity to amantadine that is found in our study.

In analyzing the results, it was not possible to correlate the attenuation in the pH activation for some mutants reported previously^{24,25} to the binding affinities that were measured in the current study. For example, the mutant A30T, which exhibits such an attenuation²⁴ has lost its ability to bind amantadine according to our studies. However, another mutant that has lost its affinity to amantadine, S31N, does not show any attenuation in its pH activation response.²⁴ Finally, another mutation that shows no attenuation in its pH activation response, V27A, does retain its amantadine

binding activity. Thus, no correlation between affinity as measured in the present study and attenuation in pH activation^{24,25} can be made.

Interestingly, a correlation can be made between the activity of the mutated ion channel and the mode of resistance. Mutants that have lost the ability to bind amantadine due to the presumed reduction in the pore diameter, also exhibit a lower amplitude of inward current.^{24,25} In contrast, mutations that retain amantadine binding due to a presumed increase in the pore diameter, exhibit higher current amplitudes.^{24,25} Thus, changes in pore size are shown to potentially affect two parameters: blocker binding and current amplitude. A larger pore would be expected to facilitate higher currents as well as retain blocker binding, albeit without blockage. Conversely, a smaller pore would be expected to exhibit reduced currents and loss of blocker binding.

In the design of new channel blockers in general, and antivirals in particular, the implication of the above results may be significant: (1) It may be necessary to differentiate between the binding of a drug and its ability to exert influence, as the two functions are shown to be disjointed. (2) When designing a new blocker against a channel that has developed resistance, it may be necessary to increase the drug size rather than decrease it. Finally, it remains to be seen whether other channels, many of which possess significant clinical importance, have developed resistance toward their cognate blocker in this fashion. Our results emphasize the need to conduct binding studies in addition to inhibition assays, which might be more sensitive, but may not reveal all of the molecular interactions that take place between the blocker and channel.

ACKNOWLEDGMENTS

We are grateful for helpful discussion with Professors E. Moczydlowski, T. A. Cross, and H. Soreq.

REFERENCES

1. Abed Y, Bourgault AM, Fenton RJ, Morley PJ, Gower D, Owens JJ, Tisdale M, Boivin G. Characterization of 2 Influenza A(H3N2) clinical isolates with reduced susceptibility to neuraminidase inhibitors due to mutations in the hemagglutinin gene. *J Infect Dis* 2002;186:1074–1080.
2. Molla A, Kati W, Carrick R, Steffy K, Shi Y, Montgomery D, Gusick N, Stoll, VS, Stewart KD, Ng TI, Maring C, Kempf DJ, Kohlbrenner, W. In vitro selection and characterization of Influenza A (A/N9) virus variants resistant to a novel neuraminidase inhibitor, A-315675. *J Virol* 2002;76:5380–5386.
3. Englund JA. Antiviral therapy of influenza. *Semin Pediatr Infect Dis* 2002;13:120–128.
4. Lamb RA, Lai CJ, Choppin PW. Sequences of mRNAs derived from genome RNA segment 7 of influenza virus: colinear and interrupted mRNAs code for overlapping proteins. *Proc Natl Acad Sci USA* 1981;78:4170–4174.
5. Parks GD, Hull JD, Lamb RA. Transposition of domains between the M2 and HN viral membrane proteins results in polypeptides which can adopt more than one membrane orientation. *J Cell Biol* 1989;109:2023–2032.
6. Sakaguchi T, Tu Q, Pinto LH, Lamb RA. The active oligomeric state of the minimalistic influenza virus M2 ion channel is a tetramer. *Proc Natl Acad Sci USA* 1997;94:5000–5005.
7. Pinto LH, Holsinger LJ, Lamb RA. Influenza virus M2 protein has ion channel activity. *Cell* 1992;69:517–528.
8. Wang C, Lamb RA, Pinto LH. Activation of the M2 ion channel of influenza virus: a role for the transmembrane domain histidine residue. *Biophys J* 1995;69:1363–1371.
9. Hay AJ, Wolstenholme AJ, Skehel JJ, Smith MH. The molecular basis of the specific anti-influenza action of amantadine. *EMBO J* 1985;4:3021–3024.
10. Kovacs FA, Cross TA. Transmembrane four-helix bundle of Influenza A M2 protein channel: structural implications from helix tilt and orientation. *Biophys J* 1997;73:2511–2517.
11. Kovacs FA, Denny JK, Song Z, Quine JR, Cross TA. Helix tilt of the M2 transmembrane peptide from Influenza A virus: an intrinsic property. *J Mol Biol* 2000;295:117–125.
12. Wang J, Kim S, Kovacs F, Cross TA. Structure of the transmembrane region of the M2 protein H(+) channel. *Protein Sci* 2001;10:2241–2250.
13. Kukol A, Adams PD, Rice LM, Brunger AT, Arkin TI. Experimentally based orientational refinement of membrane protein models: A structure for the Influenza A M2 H+ channel. *J Mol Biol* 1999;286:951–962.
14. Nishimura K, Kim S, Zhang L, Cross TA. The closed state of a H+ channel helical bundle combining precise orientational and distance restraints from solid state NMR. *Biochemistry* 2002;41:13170–13177.
15. Cooper MA, Hansson A, Lofas S, Williams DH. A vesicle capture sensor chip for kinetic analysis of interactions with membrane-bound receptors. *Anal Biochem* 2000;277:196–205.
16. Frostell-Karlsson A, Remaeus A, Roos H, Andersson K, Borg P, Hamalainen M, Karlsson R. Biosensor analysis of the interaction between immobilized human serum albumin and drug compounds for prediction of human serum albumin binding levels. *J Med Chem* 2000;43:1986–1992.
17. Duff KC, Ashley RH. The transmembrane domain of Influenza A M2 protein forms amantadine-sensitive proton channels in planar lipid bilayers. *Virology* 1992;190:485–489.
18. Wang C, Takeuchi K, Pinto LH, Lamb RA. Ion channel activity of Influenza A virus M2 protein: characterization of the amantadine block. *J Virol* 1993;67:5585–5594.
19. Smart OS, Neduveilil JG, Wang X, Wallace BA, Sansom MS. HOLE: a program for the analysis of the pore dimensions of ion channel structural models. *J Mol Graph* 1996;14:354–360.
20. Tang Y, Zaitseva F, Lamb RA, Pinto LH. The gate of the influenza virus M2 proton channel is formed by a single tryptophan residue. *J Biol Chem* 2002;277:39880–39886.
21. Sansom MS, Kerr ID, Smith GR, Son HS. The Influenza A virus M2 channel: a molecular modeling and simulation study. *Virology* 1997;233:163–173.
22. Smondyrev AM, Voth GA. Molecular dynamics simulation of proton transport through the Influenza A virus M2 channel. *Biophys J* 2002;83:1987–1996.
23. Chang NS, French RJ, Lipkind GM, Fozzard HA, Dudley S Jr. Predominant interactions between mu-conotoxin Arg-13 and the skeletal muscle Na+ channel localized by mutant cycle analysis. *Biochemistry*, 1998;37:4407–4419.
24. Holsinger LJ, Nichani D, Pinto LH, Lamb RA. Influenza A virus M2 ion channel protein: a structure-function analysis. *J Virol* 1994;68:1551–1563.
25. Grambas S, Bennett MS, Hay AJ. Influence of amantadine resistance mutations on the pH regulatory function of the M2 protein of Influenza A viruses. *Virology* 1992;191:541–549.
26. Humphrey W, Dalke A, Schulten K. VMD: visual molecular dynamics. *J Mol Graph* 1996;14:33–38.

APPENDIX

The model used to analyze the SPR data, assumed a 1:1 binding stoichiometry between amantadine and M2TMP, as reported previously:



whereby [Am] is the amantadine concentration, [M2] is the M2TMP concentration and [Am · M2] is the amantadine-M2TMP complex concentration. Eq. (2) describes the change in the concentration of the amantadine M2TMP complex, [Am · M2] as a function of time:

$$\frac{d[\text{Am}\cdot\text{M2}]}{dt} = k_{\text{on}}[\text{Am}]\cdot[\text{M2}] - k_{\text{off}}[\text{Am}\cdot\text{M2}], \quad (2)$$

whereby k_{on} and k_{off} are the association and dissociation rate constants, respectively.

Translating Eq. (2) into the SPR measurable units, we can follow the increase of $[\text{Am}\cdot\text{M2}]$ by the increase of RU as follows:

$$\frac{d\text{RU}}{dt} = k_{\text{on}}[\text{Am}]\cdot[\text{RU}_{\text{MAX}} - \text{RU}(t)] - k_{\text{off}}\text{RU}(t), \quad (3)$$

where RU_{MAX} is the RU when all the M2TMP channels are saturated with amantadine. In a state of equilibrium, the

change in RU is zero ($\frac{d\text{RU}}{dt} = 0$); thus we can describe the equilibrium RU as

$$\text{RU}_{\text{eq}} = \frac{KA\cdot[\text{Am}]\cdot\text{R}_{\text{MAX}}}{1 + KA\cdot[\text{Am}]}, \quad (4)$$

where the association constant is given by $KA = \frac{k_{\text{on}}}{k_{\text{off}}}$. This equation describes the dependence of RU_{eq} on the amantadine concentration. Thus, the dissociation constant, $KD = KA^{-1}$ can be deduced from a diagram of RU_{eq} as a function of amantadine concentrations.